JOURNAL OF MOLECULAR SPECTROSCOPY **102,** 89–111 (1983)

# Study of the Torsion-Rotation Hamiltonian for Symmetric Tops Using the Millimeter Wave Spectrum of Methyl Silane

MAN WONG[1] AND IRVING OZIER[2]

*Department of Physics, University of British Columbia, 6224 Agriculture Road, Vancouver V6T 2A6, Canada*

AND

W. LEO MEERTS

*Fysisch Laboratorium, Katholieke Universiteit, Toernooiveld, 6525 ED Nijmegen, The Netherlands*

The torsion-rotation Hamiltonian for symmetric tops has been tested in methyl silane by combining recent anticrossing molecular beam measurements in the ground torsional state ($v = 0$) with pure rotational spectra taken for $v$ as high as 4. The earlier microwave data set which consisted of $J = 1 \leftarrow 0$ and $2 \leftarrow 1$ has been greatly extended by studying millimeter transitions for $J = 4 \leftarrow 3$, $5 \leftarrow 4$, and $13 \leftarrow 12$. An analysis of the 72 rotational frequencies for $v \leq 2$ and the 15 anticrossing data for $v = 0$ yielded an excellent fit using 14 rotational, torsional, and distortion constants including the effective values for the $A$ rotational constant and the barrier height $V_3$. No satisfactory fit could be obtained when the data set was extended to include measurements for ($v = 3$) or ($v = 4$). For each of these higher torsional levels, the difference between the observed frequencies and the predictions based on the best ($v \leq 2$) constants can be expressed in terms of a shift $\delta B_v$ in the $B$ rotational constant, where $\delta B_v$ is a smooth function of the torsional energy. This disagreement is of particular interest because it may result from the fact that the molecule passes from hindered to free rotation as $v$ is increased from 2 to 4. The possibility of perturbation by a low-lying vibrational level is considered briefly. The information contained in the different types of spectra is discussed; the redundancy relations are treated and a Fourier expansion of the diagonal torsional matrix elements is introduced. For $^{12}CH_3{}^{29}SiH_3$, $^{12}CH_3{}^{30}SiH_3$, and $^{13}CH_3{}^{28}SiH_3$, pure rotational spectra for $v = 0$ were studied briefly in natural abundance. The results were combined with existing data for two deuterated symmetric rotors to obtain a structure based only on symmetric top rotational constants.

## I. INTRODUCTION

The study of internal rotation in symmetric tops has long been seriously hampered by a lack of precision experimental methods. Because of the ($\Delta K = 0$) selection rule for electric dipole transitions, the conventional microwave rotational spectrum is insensitive to the leading term in the torsional Hamiltonian. Until very recently (*1*), no direct measurement of these terms had been made and symmetric top studies had to rely on indirect techniques.

[1] Present address: Canada Centre for Remote Sensing, Ottawa K1A 0Y7, Canada.

[2] On leave (1982–1983) at the Herzberg Institute of Astrophysics, National Research Counsel of Canada, Ottawa K1A 0R6, Canada.



0022-2852/83 $3.00

The most widely used of these established methods is the torsional satellite technique introduced by Kivelson (*2*). Centrifugal distortion effects in the leading torsional terms do enter the rotational spectrum and produce splittings that, at least in higher torsional states, can be resolved with conventional microwave spectrometers. This method has now been used for several symmetric rotors including $CH_3SiF_3$ (*3, 4*), $CF_3SiF_3$ (*5*), $CF_3GeH_3$ (*6*), and $CH_3SnH_3$ (*7*).

The main weakness in this approach is that the height and shape of the potential enter only through their effect on the torsional wavefunctions used in calculating the distortional perturbations. A second difficulty lies in the fact that the results are dependent on the structure assumed. The moments of inertia about the symmetry axis of both the top ($I_\alpha$) and the entire molecule ($I_a$) are required and generally cannot be determined directly. As a result, the same data can often be interpreted in different ways, as has been done with methyl silane (*8, 9*).

With the recent development of the avoided-crossing molecular beam technique (*10, 11*), it is now possible (*1*) to measure directly in the same experiment both the leading torsional terms and the required moments of inertia. To date these measurements have been restricted to the ground torsional state. The technique has been applied to methyl silane, the prototype of the torsional satellite method. In Paper I of the current series,[3] the necessary Stark measurements were made; in Paper II,[4] the avoided-crossing results were reported and analyzed together with a molecular-beam measurement of the ($J = 1 \leftarrow 0$) rotational spectrum for the torsional state ($v = 0$) and Hirota's microwave data (*8*) for ($v = 1$) and ($v = 2$).

The purpose of the present work is to test the existing model (*2, 3*) for internal rotation in symmetric tops. To this end, the microwave data set for $^{12}CH_3{}^{28}SiH_3$ has been greatly extended; a detailed study has been carried out in the millimeter wave region covering $J = 4 \leftarrow 3$, $5 \leftarrow 4$, and $13 \leftarrow 12$, all with $v \leqslant 4$. In addition, the precision of some of the older ($J = 1 \leftarrow 0$) microwave measurements has been improved.

On the basis of this test, it is concluded that the model for internal rotation is consistent with the data from the two different techniques for the lower torsional levels ($v \leqslant 2$), but the model must be modified when the higher torsional levels ($v \geqslant 3$) are included. When 72 rotational frequencies for $v \leqslant 2$ and 15 anticrossing data for $v = 0$ are analyzed, an excellent fit is obtained using 14 rotational, torsional, and distortion constants; the results are listed in Table I. However, for ($v = 3$) and ($v = 4$), a clear discrepancy exists between the measurements and the frequencies predicted from Table I. For ($v = 3$), this discrepancy can be expressed as $2\delta B_3(J + 1)$, where $\delta B_3$ is a smooth function of the torsional energy $E_T^{(0)}$. Similar behavior is observed for ($v = 4$), although $\delta B_4$ is less sensitive to $E_T^{(0)}$. Regardless of which torsion–rotation parameters are added to those listed in Table I and regardless of the values used for the entire set, the differences between the observed and calculated frequencies remain an order of magnitude larger than the experimental errors.

Two possible mechanisms for the disagreement between experiment and theory are suggested. The first involves a torsional perturbation which is enhanced by the

[3] Paper I refers to Ref. (*12*).

[4] Paper II refers to Ref. (*13*).

TABLE I

Molecular Constants for $CH_3{}^{28}SiH_3$[a]

| Quantity | | Value | |
|---|---|---|---|
| $A^{eff}$ | (MHz) | 56 189.167 | (17) |
| B | (MHz) | 10 986.0949 | (51) |
| $D_J$ | (kHz) | 10.7111 | (95) |
| $D_{JK}$ | (kHz) | 45.550 | (57) |
| $D_K$ | (kHz) | 189.65[b] | |
| $\rho$ | | 0.351 8124 | (49) |
| $V_3^{eff}$ | ($cm^{-1}$) | 592.3334 | (72) |
| $F_{3J}$ | (MHz) | -135.77 | (17) |
| $F_{6J}$ | (MHz) | -4.83 | (14) |
| $D_{Jm}$ | (MHz) | 0.6714 | (78) |
| $D_{Km}^{eff}$ | (MHz) | 10.7 | (1.9) |
| $d_J$ | (MHz) | -0.1257 | (13) |
| $H_{Jmm}$ | (Hz) | 670. | (160) |
| $H_{JKm}$ | (Hz) | -59. | (10) |
| $H_{JJm}$ | (Hz) | 10.14 | (70) |

a - Several quartic and sextic constants were fixed at zero. See text.

b - This is fixed at the force field value (23).

passage of the molecule from hindered rotation ($v \leqslant 2$) to free rotation ($v \geqslant 4$). The second involves a vibration–torsion–rotation perturbation by the nearby lowest-lying degenerate vibrational level ($v_{12} = 1$) and/or the associated sequence of torsional combination levels. The nature of this mechanism is important not only with respect to the modifications needed in this model, but also with respect to the properties deduced for other molecules which undergo internal rotation.

In establishing that the model behaves as described, the development of the torsion–rotation Hamiltonian is outlined briefly with emphasis on the redundancy relations (*14, 15*) and the problem of extracting the true values of the leading parameters from the experimental data. The information contained first in the torsional satellite spectra and second in the anticrossing measurements is discussed. In treating the latter, the standard Fourier analysis (*16*) used for internal rotation is extended; the resulting expansions lead to the formulas for the effective parameters introduced in Paper II (*13*).

Rotational spectra for ($v = 0$) were obtained for three modifications: $^{12}CH_3{}^{30}SiH_3$, $^{12}CH_3{}^{29}SiH_3$, and $^{13}CH_3{}^{28}SiH_3$. The first of these was studied to complement the anticrossing measurements on this isotopic form in Paper II (*13*). The data on the

four isotopic modifications studied here were combined with results from earlier experiments on $^{12}CH_3{}^{28}SiD_3$ (*8*) and $^{12}CD_3{}^{28}SiH_3$ (*9*) to obtain the structure from symmetric top measurements only.

In the current work, the notation will follow as closely as possible that used in Papers I and II. Definitions not given explicitly here can be taken over from these earlier works. The fundamental constants are taken from Ref. (*17*).

## II. THEORETICAL BACKGROUND

### *1. The Hamiltonian*

To establish that theory and experiment do not agree, care must be taken that all relevant terms in the torsion–rotation Hamiltonian $H_{TR}$ are included. In the current work the internal-axis method (IAM) is used.[5] One starts with a classical formulation of the hindered rotor problem and obtains the quantum mechanical Hamiltonian $H_{TR}^{PAM}$ in the principal-axis method (PAM) (*3, 16*). The IAM Hamiltonian $H_{TR}$ is then obtained in a process which involves the transformation of the torsional angular momentum

$$\mathbf{p}_{PAM} = \mathbf{p} + \rho \mathbf{J}_z. \tag{1}$$

In zeroth order, $H_{TR}^{PAM}$ contains the term $-2A'\mathbf{J}_z\,\mathbf{p}_{PAM}$ where $A'$ is the rotational constant of the silyl frame. In zeroth order, $H_{TR}^{IAM}$ contains no coupling term between $\mathbf{J}_z$ and $\mathbf{p}$; the term is eliminated by setting

$$\rho = I_\alpha / I_a. \tag{2}$$

The zeroth order IAM Hamiltonian $H_{TR}^{(0)}$ can then be written as the sum of a rotational term $H_R^{(0)}$ and a torsional term $H_T^{(0)}$ where

$$H_R^{(0)} = B\mathbf{J}^2 + (A - B)\mathbf{J}_z^2; \tag{3a}$$

$$H_T^{(0)} = F\mathbf{p}^2 + V_3 \frac{1}{2}(1 - \cos 3\alpha). \tag{3b}$$

The reduced rotational constant

$$F \equiv A/[\rho(1 - \rho)]. \tag{4}$$

In this order, $V_3$ is the height of the threefold potential $V(\alpha)$.

In extending the calculation of $H_{TR}$ beyond zeroth order, it is convenient to consider the Fourier factor $(1 - \cos 3n\alpha)/2$ with $n = 1, 2, 3, \ldots$ to be of the same order as a factor of degree $2n$ in the angular momenta. Then the first-order Hamiltonian

$$H_{TR}^{(1)} = V_6 \frac{1}{2}(1 - \cos 6\alpha) + \zeta\mathbf{p}^2 + \frac{1}{2}(1 - \cos 3\alpha)[F_{3J}\mathbf{J}^2 + F_{3K}\mathbf{J}_z^2] - D_J\mathbf{J}^4$$

$$- D_{JK}\mathbf{J}^2\mathbf{J}_z^2 - D_K\mathbf{J}_z^4 - [D_{Jm}\mathbf{J}^2 + D_{Km}\mathbf{J}_z^2 + D_m\mathbf{p}^2]\mathbf{p}^2 - [d_J\mathbf{J}^2 + d_K\mathbf{J}_z^2 + d_m\mathbf{p}^2]\mathbf{J}_z\mathbf{p}$$

[5] When the notation does not explicitly indicate the coordinate system, it is understood that the IAM is to be used.

$$+ f_3[\mathbf{J}_z\mathbf{p}\cos 3\alpha + \cos 3\alpha\,\mathbf{J}_z\mathbf{p}] + F_{3m}\left[\mathbf{p}^2\frac{1}{2}(1-\cos 3\alpha) + \frac{1}{2}(1-\cos 3\alpha)\,\mathbf{p}^2\right]. \quad (5)$$

The division between $H_{TR}^{(0)}$ and $H_{TR}^{(1)}$ is somewhat arbitrary; the particular division described here (termed Method I) is that commonly used in the literature (*14, 16, 18*). An alternative method is described here in Section II.3. The parameters $F_{3J}$, $D_{Jm}$, and $d_J$ are related in Paper II to the older notation (*2, 3, 8, 14*). The constants $k_1$, $k_2$, $k_3$, $k_4$, $k_5$, and $k_7$ used in Refs. (*14*) and (*18*) are here denoted, respectively, by $-d_K$, $-D_{Km}$, $-d_m$, $-D_m$, $(1/2)F_{3K}$, and $F_{3m}$. In the current notation, the operation associated with each constant can be read from the constant itself once two rules are defined. First, an $F_{3n}$ (or $f_{3n}$) involves a Fourier factor $\cos 3n\alpha$, while a $D$ (or $d$) does not. Second, a lower case implies an operator $\mathbf{J}_z\mathbf{p}$ in addition to the operators specified by the subscripts. These rules clearly do not apply to $V_3$ or $\zeta$.

In the current work, the coupling term $\mathbf{J}_z\mathbf{p}$ is absent from $H_{TR}$ in first order as well. This is achieved by replacing $\rho$ in Eq. (1) by an effective value $\tilde{\rho}$. To see how $\tilde{\rho}$ differs from $\rho$, it is necessary to consider the terms in the first-order PAM Hamiltonian which can produce a term $\mathbf{J}_z\mathbf{p}$ in $H_{TR}$. These are

$$H'_{PAM} = \epsilon\mathbf{J}_z\mathbf{p}_{PAM} + \epsilon'\left[\mathbf{J}_z\mathbf{p}_{PAM}\frac{1}{2}(1-\cos 3\alpha) + \frac{1}{2}(1-\cos 3\alpha)\mathbf{J}_z\mathbf{p}_{PAM}\right]$$
$$+ \epsilon''\left[\mathbf{p}_{PAM}^2\frac{1}{2}(1-\cos 3\alpha) + \frac{1}{2}(1-\cos 3\alpha)\mathbf{p}_{PAM}^2\right]. \quad (6)$$

$\epsilon$ arises from inertial defect effects (*19*). It was found to be significant in both nitromethane (*19*) and methyl alcohol (*14*). It can be shown that

$$\epsilon'' = F_{3m}; \quad (7a)$$

$$\epsilon' = f_3 - 2\rho F_{3m}. \quad (7b)$$

Then

$$\tilde{\rho} = \rho - [\epsilon + f_3 - \rho F_{3m}]/F. \quad (8a)$$

These terms in $H'_{PAM}$ also make a contribution to $H_{TR}$ of the form $\mathbf{J}_z^2$, so that $A$ in Eq. (3) must be replaced by

$$\tilde{A} = A + \rho\epsilon. \quad (8b)$$

Similarly, the coefficient of $(1/2)(1-\cos 3\alpha)\mathbf{J}_z^2$ is modified to form $\tilde{F}_{3K}$. Since neither $A$ nor $\rho$ can be isolated, $F$ must be taken as

$$\tilde{F} = \tilde{A}/[\tilde{\rho}(1-\tilde{\rho})]. \quad (9)$$

To correct for this, the term in $\mathbf{p}^2$ is introduced in Eq. (5) with $\zeta \equiv (F - \tilde{F})$. Equations (7) and (8) are accurate only to first order in the quartic constants $\epsilon$, $f_3$, and $F_{3m}$.

Because rather high values of $J$ have been investigated, the next order contribution to the Hamiltonian must be included:

$$H_{TR}^{(2)} = V_9\frac{1}{2}(1-\cos 9\alpha) + \frac{1}{2}(1-\cos 6\alpha)[F_{6J}\mathbf{J}^2 + F_{6K}\mathbf{J}_z^2] + \frac{1}{2}(1-\cos 3\alpha)$$
$$\times [G_{3JJ}\mathbf{J}^4 + G_{3JK}\mathbf{J}^2\mathbf{J}_z^2 + G_{3KK}\mathbf{J}_z^4] + H_{JJJ}\mathbf{J}^6 + H_{JJK}\mathbf{J}^4\mathbf{J}_z^2 + H_{JKK}\mathbf{J}^2\mathbf{J}_z^4 + H_{KKK}\mathbf{J}_z^6$$

$$+ [H_{JJm}\mathbf{J}^4 + H_{JKm}\mathbf{J}^2\mathbf{J}_z^2 + H_{KKm}\mathbf{J}_z^4]\mathbf{p}^2 + [H_{Jmm}\mathbf{J}^2 + H_{Kmm}\mathbf{J}_z^2 + H_{mmm}\mathbf{p}^2]\mathbf{p}^4$$
$$+ [h_{JJ}\mathbf{J}^4 + h_{JK}\mathbf{J}^2\mathbf{J}_z^2 + h_{KK}\mathbf{J}_z^4]\mathbf{J}_z\mathbf{p} + [h_{Jm}\mathbf{J}^2 + h_{Km}\mathbf{J}_z^2 + h_{mm}\mathbf{p}^2]\mathbf{J}_z p^3. \quad (10)$$

Equation (10) omits all terms involving the factor $(1/2)(1 - \cos 3n\alpha)\mathbf{p}$ or $\mathbf{p}(1/2)(1 - \cos 3n\alpha)$. They are redundant in the sense defined in Section II.2. and will contribute no more than a correction in the next highest order.

*2. The Energies*

The total torsion–rotation energy $E$ for a symmetric top in the ground vibronic state can be labeled by the quantum numbers $(v, J, K, \sigma)$. For each torsional level $v$, the sublevels of symmetry $A$ and $E$ are labeled by $(\sigma = 0)$ and $(\sigma = \pm 1)$, respectively. The correspondence between the torsion–rotation symmetry $\Gamma$ and $(J, K, \sigma)$ is given in Ref. (*8*).

In Method I, the zeroth-order energy $E_0(v, J, K, \sigma)$ is obtained by first diagonalizing $H_T^{(0)}$ to obtain the torsional contribution $E_T^{(0)}$ and then adding the rotational contribution $E_R^{(0)}$. See Eq. (3). The torsion-rotation eigenfunctions of $H_{TR}^{(0)}$ are referred to as Basis I. The first-order correction $E_1(v, J, K, \sigma)$ can be read directly from Eq. (5) by replacing each operator $\Omega$ by its diagonal matrix element $\langle\Omega\rangle_{vK\sigma}$ calculated by this basis.

A careful selection of independent parameters must be made in a first-order calculation from among $V_3$, $V_6$, $A$, $\rho$, $F$, $\zeta$, $f_3$, and $F_{3m}$. In doing so, account must be taken of two "redundancy" relations (*14*). First,

$$\langle\mathbf{p}\cos 3\alpha\rangle_{vK\sigma} = \langle\cos 3\alpha\ \mathbf{p}\rangle_{vK\sigma} = 0. \quad (11)$$

This eliminates $f_3$. The second relation can be read from Eq. (12) below by setting $V_6 = \zeta = D_{Km} = 0$. This shows $F_{3m}$ can be eliminated by introducing effective parameters for $\zeta$, $V_3$, and $V_6$. The effective value for $F$ is not independent since it is calculated from Eq. (*9*). In the group above, then, the independent effective values are those for $V_3$, $V_6$, $A$, $\rho$, and $\zeta$.

In the work on methyl alcohol (*14, 18*), the moments of inertia of the top and frame were used as independent parameters. Here $A$ and $\rho$ are used instead. This choice was dictated by the nature of the anticrossing experiments; see Section IV. Because $H_{TR}^{(1)}$ contains no term in $\mathbf{J}_z\mathbf{p}$, the treatment here is equivalent to setting $k_6$ in Ref. (*14*) to zero; a first-order analysis with Method I thus corresponds to Fit I of Lees and Baker (*14*).

The second-order energy $E_2(v, J, K, \sigma)$ consists of two parts: the diagonal matrix elements of $H_{TR}^{(2)}$ and the second-order perturbation sums due to $H_{TR}^{(1)}$. In the latter, the contributions from $f_3$ and $F_{3m}$ must be included since the two redundancy relations apply only to the diagonal matrix elements. Of course, higher-order redundancy relations exist (*15*), so that not all the different contributions to $E_2(v, J, K, \sigma)$ can be isolated. However, since the current data set can fix at most four sextic constants, no attempt was made to pursue this question.

The calculation in Method I of the second-order correction due to $H_{TR}^{(1)}$ is very awkward. Not only are there a large number of terms, but many of these can be rather large, particularly those involving $V_6$ and $\zeta$. These constants can lead to $J$-dependent contributions through various cross terms.

To simplify the calculation, Method II was introduced in which all the $J$-independent torsional terms in Eq. (5) were transferred from $H_{TR}^{(1)}$ into $H_T^{(0)}$ to define a new zeroth-order torsional Hamiltonian $\tilde{H}_T^{(0)}$, as well as corresponding new zeroth- and first-order torsion–rotation Hamiltonians $\tilde{H}_{TR}^{(0)}$ and $\tilde{H}_{TR}^{(1)}$, respectively. The eigenfunctions of $\tilde{H}_{TR}^{(0)}$ form Basis II. By isolating the $J$-dependent distortion terms in $\tilde{H}_{TR}^{(1)}$ in this way, the number of terms in the perturbation sums and their magnitude were greatly reduced without increasing the dimensionality of the torsional matrix to be diagonalized.

This change of basis, however, requires that the redundancy relations be reconsidered because they were derived (*14*) only for Basis I. If *only* the terms in $V_6$, $\zeta$, and $D_{Km}$ are included in the transfer, then redundancy relation (11) is not altered. Furthermore, the second relation can be written

$$\left\langle \mathbf{p}^2 \frac{1}{2}(1 - \cos 3\alpha) + \frac{1}{2}(1 - \cos 3\alpha)\,\mathbf{p}^2 \right\rangle_{vK\sigma}$$

$$= \langle \mathbf{p}^2 \rangle_{vK\sigma} + \left(\frac{9}{2} + \frac{V_6}{2F'}\right)\left\langle \frac{1}{2}(1 - \cos 3\alpha) \right\rangle_{vK\sigma} - (V_3/4F')\left\langle \frac{1}{2}(1 - \cos 6\alpha) \right\rangle_{vK\sigma}$$

$$- (V_6/2F')\left\langle \frac{1}{2}(1 - \cos 9\alpha) \right\rangle_{vK\sigma} - 9/4 \quad (12a)$$

where

$$F' = \tilde{F} + \zeta - K^2 D_{Km}. \quad (12b)$$

In this case, to first order, $f_3$ can be dropped and $F_{3m}$ can be eliminated by introducing the effective parameters

$$\tilde{\zeta} = \zeta + F_{3m} \quad (13a)$$

$$\tilde{V}_3 = V_3 + (9/2 + V_6/2F)F_{3m} \quad (13b)$$

$$\tilde{V}_6 = V_6 - F_{3m}V_3/4F. \quad (13c)$$

In addition, $\tilde{V}_9$ must be introduced and the meaning of $\tilde{F}_{3K}$ is altered.

In applying Method II, this form of the redundancy relation is used, thus eliminating diagonal contributions of $f_3$ and $F_{3m}$. Because the transfer included more than just $V_6$, $\zeta$, and $D_{Km}$, this step introduces an error. However, because $V_6$ and $\zeta$ are dominant, the error is insignificant. Furthermore, the off-diagonal terms of $f_3$ and $F_{3m}$ can be neglected.

In the final fit, $V_6$ and $\zeta$ were fixed at zero so that the most important differences between Methods I and II are discarded in the end. In spite of this, Method II is very useful: in the calculations which establish that in fact only the constants given in Table I can be determined, the simplifications inherent in Method II are very helpful. Method II will prove even more useful in analyzing later experiments in which $\tilde{V}_6$ and $\tilde{\zeta}$ can be determined.

Direct diagonalization (Method III) was also used. As in Method II, the simplifications from the redundancy relations were used and $f_3$ with $F_{3m}$ were eliminated without correction. Aside from this, the full torsion–rotation Hamiltonian was diagonalized for each relevant value of $J$. No significant difference could be found

between Methods II and III. Once this was established, Method II was used routinely and Method III was applied only to obtain the final fit.

## III. THE ROTATIONAL SPECTRUM

The electric dipole selection rules for the rotational spectra observed are $(J' - J) = \Delta J = 1$, $\Delta K = 0$, $\Delta\sigma = 0$. In Method II, the frequencies for these transitions can be written to sextic degree as

$$\nu(v, J, K, \sigma) = 2(J + 1)\hat{B}(v, K, \sigma) - 2(J + 1)K^2\hat{D}_{JK}(v, K, \sigma) - 4(J + 1)^3\hat{D}_J(v, K, \sigma) + H_{JJJ}(J + 1)^3\{(J + 2)^3 - J^3\}. \quad (14)$$

Here

$$\hat{B}(v, K, \sigma) = B + F_{3J}\left\langle \frac{1}{2}(1 - \cos 3\alpha)\right\rangle_{vK\sigma} + F_{6J}\left\langle \frac{1}{2}(1 - \cos 6\alpha)\right\rangle_{vK\sigma} - D_{JM}\langle \mathbf{p}^2\rangle_{vK\sigma} - d_JK\langle \mathbf{p}\rangle_{vK\sigma} + H_{Jmm}\langle \mathbf{p}^4\rangle_{vK\sigma} + h_{Jm}K\langle \mathbf{p}^3\rangle_{vK\sigma} + H_{JKK}K^4 - D_mF_{3J}\Sigma_1 + D_mD_{Jm}\Sigma_2 \quad (15)$$

where $\Sigma_1$ and $\Sigma_2$ are different second-order perturbation sums. It is implicit here that the matrix elements are to be calculated in Basis II. Expressions similar to (15) can be derived for $\hat{\mathbf{D}}_{JK}(v, K, \sigma)$ and $\hat{D}_J(v, K, \sigma)$ from Eqs. (3), (5), and (10).

For a given torsional sublevel $(v, K, \sigma)$, $\hat{B}$, $\hat{D}_{JK}$, and $\hat{D}_K$ are effective constants independent of $J$ because the matrix elements and the second-order corrections are not functions of $J$. The basis of the torsional satellite method lies in the fact that the effective rotational constant $\hat{B}$ for *all* the sublevels can be accounted for by a single expression, namely (15), where all the matrix elements can be calculated from the eigenfunctions of the same torsional Hamiltonian. The effective quartic distortion constants $\hat{D}_{JK}$ and $\hat{D}_K$ can be calculated in a similar way, but their changes with $(v, K, \sigma)$ are much smaller.

The microwave spectrum of $CH_3{}^{28}SiH_3$ was first reported by Lide and Coles (*20*), who observed the $(J_K = 1_0 \leftarrow 0_0)$ spectrum in the 21-GHz region. This particular spectrum was subsequently remeasured by Hirota (*8*) and by Ewig *et al.* (*9*). In Paper II, the very small $\sigma$ splitting in the $(v = 0)$ state was partially resolved with a molecular beam spectrometer. Hirota (*8*) extended the microwave measurements to the $(J_K = 2_1 \leftarrow 1_1)$ spectrum.

In the present experiment, four different $(J + 1 \leftarrow J)$ spectra were studied, all at room temperature. Three lines in the $(J = 1 \leftarrow 0)$ spectrum with $v \geq 2$ were measured once more to reduce the errors to 30 kHz. The values agreed with the older determinations. To test the accuracy, the ground state $(J = 1 \leftarrow 0)$ line was observed. The resulting frequency of 21 931.901 (20) MHz for the unresolved pattern was within 5 kHz of the value calculated from the Paper II beam measurements of the partially resolved spectrum. The current observations were made with a conventional Stark-modulated spectrometer in the Department of Chemistry at the University of British Columbia. To improve the sensitivity, a 6-m $X$-band absorption cell was used with a phase-locked klystron source swept by a signal averager.

The $(J = 4 \leftarrow 3)$ and $(J = 5 \leftarrow 4)$ transitions were studied with the computer-

controlled millimeter wave spectrometer in the Department of Physics at the University of British Columbia. The basic instrument as described by Statt *et al.* (*21*) was modified for Stark spectroscopy with conventional techniques. A 3-m $K$ band absorption cell was used. The source was a phase-locked backward wave oscillator. The linewidth was typically 700 kHz.

The ($J = 13 \leftarrow 12$) spectrum in the 285-GHz region was studied with the millimeter wave spectrometer (*22*) in the Institut für Molekülphysik of the Freie Universität, Berlin. Because saturation modulation was used, the lines with $K = 0$ could be observed. A 1-m free space absorption cell was employed. The source was a phase-locked carcinotron. The lines had a width of 650 kHz.

The frequencies obtained for $v \leqslant 2$, $v = 3$, and $v = 4$ are listed in Tables II, III, and IV, respectively. In most cases, the frequency was measured at least twice. Also included in these tables are the earlier measurements (*8, 14*) for lines which were not studied in the current work.

For each ($J + 1 \leftarrow J$), the distribution of the frequencies with ($v$, $K$, $\sigma$) shows a similar pattern which is strongly affected by the fact that the torsional energy $E_T^{(0)}$ is clearly $< V_3$ for $v \leqslant 2$, $E_T^{(0)} \sim V_3$ for $v = 3$, and $E_T^{(0)}$ is clearly $> V_3$ for $v \geqslant 4$. Consider the $J = (4 \leftarrow 3)$ spectrum as an example of the pattern. For ($v \leqslant 3$), the spectrum consists of sets of well-separated lines, one set for each $v$. The spread within each set due to the ($K$, $\sigma$) dependence of $\nu(v, J, K, \sigma)$ increases with $v$ from $\sim$3 MHz for ($v = 0$) to $\sim$40 MHz for ($v = 3$). The separation between sets decreases with $v$; the gap between ($v = 0$) and ($v = 1$) is 260 MHz, while that between ($v = 2$) and ($v = 3$) is only 170 MHz.

For $v > 3$ where the levels are well above the top of the barrier, these characteristics change. The effect of the potential $V(\alpha)$ on $\hat{B}$, $\hat{D}_{JK}$, and $\hat{D}_J$ is greatly reduced and the lines no longer separate into distinct sets according to $v$. Calculations show that lines for $v = 4$ and 5 are closely intermingled. At room temperature, the predicted intensities of the strongest ($v = 5$) lines are comparable to the intensities of the intermediate ($v = 4$) lines. Thus the identification of the lines for $v > 3$ is very difficult. The procedure used here is discussed in Section V. *It should be emphasized that the identification given in Table IV for $v = 4$ is tentative.*

A torsional satellite study such as that described here can yield $B$ and the quartic distortion constants that enter in Eq. (14) provided enough torsional sublevels are studied to sufficient accuracy. The sextic constants are treated here entirely empirically, in part because of the question of higher-order redundancy relations. The sextic constants are included primarily to improve the values of the quartic parameters.

## IV. THE ANTICROSSING MEASUREMENTS

A description of the molecular beam studies of both the barrier and rotational anticrossings was given in Paper II, but it was left to the current work to determine in detail how much information can be extracted from these data. To answer this question, we will first extend the standard Fourier analysis (*16*) that has been used in internal rotor problems. Since all the data were in the ground torsional state with low $J$ and $K$, the sextic terms will not be considered.

It is well known (*16*) that in Method I the eigenvalues $E_T^{(0)}$ of the zeroth-order Hamiltonian $H_T^{(0)}$ can be expanded as

TABLE II

Pure Rotational Frequencies (in MHz) for $CH_3{}^{28}SiH_3$ in Torsional Levels well below the Barrier Top

| Lower State | | | | Observed Value[b] | δ ≡ Observed -Calculated |
|---|---|---|---|---|---|
| v | J | K | σ[a] | | |
| 0 | 0 | 0 | 0 | 21 937.885 (010)[c] | -0.001 |
| 0 | 0 | 0 | ±1 | 21 937.913 (010)[c] | 0.002 |
| 1 | 0 | 0 | 0 | 21 873.100 (100)[d] | 0.034 |
| 1 | 0 | 0 | ±1 | 21 872.460 (100)[d] | 0.089 |
| 2 | 0 | 0 | 0 | 21 808.928 (030) | 0.001 |
| 2 | 0 | 0 | ±1 | 21 814.465 (030) | 0.008 |
| 0 | 1 | ±1 | mean | 43 875.280 (170)[d] | -0.080 |
| 1 | 1 | ±1 | 0 | 43 745.410 (100)[d] | -0.057 |
| 1 | 1 | ±1 | ±1 | 43 744.750 (100)[d] | -0.178 |
| 1 | 1 | ±1 | ∓1 | 43 743.880 (100)[d] | -0.027 |
| 2 | 1 | ±1 | 0 | 43 618.530 (100)[d] | -0.226 |
| 2 | 1 | ±1 | ±1 | 43 622.730 (100)[d] | -0.117 |
| 2 | 1 | ±1 | ∓1 | 43 632.890 (100)[d] | -0.306 |
| 0 | 3 | ±1 | mean | 87 748.681 (050) | 0.008 |
| 0 | 3 | ±2 | mean | 87 747.601 (050) | 0.003 |
| 0 | 3 | ±3 | mean | 87 745.744 (050) | -0.034 |
| 1 | 3 | ±1 | 0 | 87 488.837 (100) | -0.065 |
| 1 | 3 | ±1 | ±1 | 87 487.828 (200) | 0.005[e] |
| 1 | 3 | ±1 | ∓1 | 87 485.750 (100) | -0.031 |
| 1 | 3 | ±2 | 0 | 87 486.537 (300) | -0.136[e] |
| 1 | 3 | ±2 | ±1 | 87 487.828 (200) | -0.006[e] |
| 1 | 3 | ±2 | ∓1 | 87 484.596 (100) | -0.098 |
| 1 | 3 | ±3 | 0 | 87 483.503 (200) | -0.093[e] |
| 1 | 3 | ±3 | ±1 | 87 486.537 (300) | 0.119[e] |
| 1 | 3 | ±3 | ∓1 | 87 483.503 (200) | -0.173[e] |
| 2 | 3 | ±1 | 0 | 87 235.518 (050) | 0.037 |
| 2 | 3 | ±1 | ±1 | 87 243.682 (050) | 0.015 |
| 2 | 3 | ±1 | ∓1 | 87 264.420 (050) | 0.044 |
| 2 | 3 | ±2 | 0 | 87 242.180 (050) | -0.083 |
| 2 | 3 | ±2 | ±1 | 87 234.680 (100) | 0.048 |
| 2 | 3 | ±2 | ∓1 | 87 263.240 (050) | 0.032 |
| 2 | 3 | ±3 | 0 | 87 251.973 (200) | -0.064[e] |
| 2 | 3 | ±3 | ±1 | 87 229.762 (100) | -0.001 |
| 2 | 3 | ±3 | ∓1 | 87 251.973 (200) | -0.106[e] |
| 0 | 4 | ±1 | mean | 109 683.947 (050) | 0.026 |
| 0 | 4 | ±2 | mean | 109 682.621 (050) | 0.043 |
| 0 | 4 | ±3 | mean | 109 680.280 (050) | -0.022 |
| 0 | 4 | ±4 | mean | 109 677.091 (050) | 0.006 |
| 1 | 4 | ±1 | 0 | 109 359.222 (100) | 0.000 |
| 1 | 4 | ±1 | ±1 | 109 357.897 (200) | 0.024[e] |
| 1 | 4 | ±2 | 0 | 109 356.408 (400) | -0.027[e] |
| 1 | 4 | ±2 | ±1 | 109 357.897 (200) | 0.010[e] |
| 1 | 4 | ±2 | ∓1 | 109 353.960 (100) | -0.001 |
| 1 | 4 | ±3 | 0 | 109 352.600 (200) | 0.012[e] |
| 1 | 4 | ±3 | ±1 | 109 356.408 (400) | 0.289[e] |
| 1 | 4 | ±3 | ∓1 | 109 352.600 (200) | -0.089[e] |

$$\langle H_T \rangle_{vK\sigma} = \sum_{n=0}^{\infty} a_n^{(E)} \cos\left[(2\pi n/3)(\tilde{\rho}K - \sigma)\right]. \tag{16}$$

The arguments leading to expansion (16) can be extended to the diagonal matrix elements of any torsional operator in either Basis I or II. For each torsional operator $\Omega_p$ of interest here, the diagonal matrix elements $\langle \Omega_p \rangle_{vK\sigma}$ are either even or odd under the operation $(K\sigma) \leftrightarrow (-K, -\sigma)$ according as $p$ is $+1$ or $-1$, respectively. In all even cases, $\langle \Omega_{+1} \rangle_{vK\sigma}$ can be expanded as in Eq. (16); for the odd cases,

TABLE II—*Continued*

| v | Lower State J | K | σ[a] | Observed Value[b] | δ ≡ Observed −Calculated |
|---|---|---|---|---|---|
| 2 | 4 | ±1 | 0 | 109 042.516 (100) | 0.069 |
| 2 | 4 | ±1 | ±1 | 109 052.682 (050) | −0.002 |
| 2 | 4 | ±1 | ∓1 | 109 078.689 (100) | 0.109 |
| 2 | 4 | ±2 | 0 | 109 050.954 (100) | 0.025 |
| 2 | 4 | ±2 | ±1 | 109 041.600 (300) | 0.215 |
| 2 | 4 | ±2 | ∓1 | 109 077.114 (100) | −0.006 |
| 2 | 4 | ±3 | 0 | 109 063.237 (200) | 0.085[e] |
| 2 | 4 | ±3 | ±1 | 109 035.145 (300) | −0.154 |
| 2 | 4 | ±3 | ∓1 | 109 063.237 (200) | 0.033[e] |
| 2 | 4 | ±4 | 0 | 109 072.017 (100) | 0.015 |
| 2 | 4 | ±4 | ±1 | 109 035.145 (300) | 0.081 |
| 2 | 4 | ±4 | ∓1 | 109 046.254 (200) | 0.132 |
| 0 | 12 | 0 | mean | 285 099.430 (150) | −0.025 |
| 0 | 12 | ±1 | mean | 285 098.370 (150) | 0.037 |
| 0 | 12 | ±2 | mean | 285 094.900 (050) | 0.058 |
| 0 | 12 | ±3 | mean | 285 088.910 (100) | −0.015 |
| 0 | 12 | ±4 | mean | 285 080.540 (100) | −0.019 |
| 0 | 12 | ±5 | mean | 285 069.870 (050) | 0.011 |
| 0 | 12 | ±6 | mean | 285 056.820 (050) | −0.009 |
| 0 | 12 | ±7 | mean | 285 041.310 (050) | −0.055 |
| 0 | 12 | ±8 | mean | 285 023.450 (050) | −0.023 |
| 0 | 12 | ±9 | mean | 285 003.170 (050) | −0.033 |
| 0 | 12 | ±10 | mean | 284 980.680 (050) | −0.010 |
| 0 | 12 | ±11 | mean | 284 955.810 (050) | −0.003 |
| 0 | 12 | ±12 | mean | 284 928.570 (050) | 0.057 |
| 1 | 12 | 0 | 0 | 284 257.520 (100) | 0.099 |
| 1 | 12 | ±1 | 0 | 284 254.750 (100) | 0.010 |
| 1 | 12 | ±1 | ±1 | 284 251.240 (200) | 0.032[e] |
| 1 | 12 | ±2 | ±1 | 284 251.240 (200) | −0.030[e] |
| 2 | 12 | 0 | ±1 | 283 496.020 (100) | 0.031 |
| 2 | 12 | ±1 | ∓1 | 283 525.660 (100) | −0.036 |
| 2 | 12 | ±2 | ∓1 | 283 521.810 (100) | −0.084 |
| 2 | 12 | ±3 | 0 | 283 485.410 (200) | 0.024[e] |
| 2 | 12 | ±3 | ∓1 | 283 485.410 (200) | −0.089[e] |
| 2 | 12 | ±4 | 0 | 283 508.620 (070) | 0.020 |
| 2 | 12 | ±5 | 0 | 283 497.120 (100) | −0.010 |

a - The entry "mean" indicates that the σ splitting was not resolved. The fit was made by setting the calculated frequency equal the average over σ weighted by the intensities.

b - Except as noted, the frequencies were measured in the current work.

c - These fequencies were taken from Paper II (13).

d - These frequencies were taken from Ref.(8). No errors were given in the original work. The error assumed in the present fit was 100 kHz for each line with one exception. For (v = 0), the error was increased to 170 kHz because of the averaging involved as mentioned in Footnote a.

e - In these cases, two different calculated frequencies lie very close to the measured value. Both identifications were accepted and the errors increased to allow for the calculated separation.

$$\langle \Omega_{-1} \rangle_{vK\sigma} = \sum_{n=1}^{\infty} a_n^{(\Omega)} \sin [(2\pi n/3)(\tilde{\rho} K - \sigma)]. \tag{17}$$

In all cases, the expansion coefficients $a_n^{(\Omega)}$ depend on only one quantum number, namely $v$. They depend, of course, on the particular operator being expanded. In Basis I, the only molecular parameter that affects the $a_n^{(\Omega)}$ is the reduced barrier height $s$. In Basis II, the $a_n^{(\Omega)}$ depend as well on the additional parameters in $\bar{H}_{TR}^{(0)}$, but this dependence is very weak.

TABLE III

Pure Rotational Frequencies for $CH_3{}^{28}SiH_3$ in the ($v$ = 3) Torsional Level

| Lower State J | K | σ | Γ | Observed Value[a] (MHz) | δ[b] (MHz) | $\delta B_3$[c] (MHz) | $E_T^{(0)} - V_3^{eff}$ ($cm^{-1}$) |
|---|---|---|---|---|---|---|---|
| 0 | 0 | 0 | $A_2$ | 21 768.727 (030) | - 6.05 | -3.03 | 21.6 |
| 0 | 0 | ±1 | $E_4$ | 21 758.47 (100)[d] | - 0.60 | -0.30 | -24.2 |
| 1 | ±1 | 0 | $E_1$ | 43 530.60 (100)[d] | - 4.86 | -1.22 | 8.3 |
| 1 | ±1 | ±1 | $E_2$ | 43 520.92 (100)[d] | - 2.44 | -0.61 | - 8.2 |
| 1 | ±1 | ∓1 | $E_3$ | 43 512.31 (100)[d] | - 0.84 | -0.21 | -32.9 |
| 3 | ±1 | 0 | $E_1$ | 87 059.670 (070)[e] | - 9.25 | -1.16 | 8.3 |
| 3 | ±1 | ±1 | $E_2$ | 87 040.273 (070)[f] | - 4.44 | -0.56 | - 8.2 |
| 3 | ±1 | ∓1 | $E_3$ | 87 022.707 (070)[f] | - 1.56 | -0.20 | -32.9 |
| 3 | ±2 | 0 | $E_1$ | 87 046.428 (070) | - 4.10 | -0.51 | -11.1 |
| 3 | ±2 | ±1 | $E_3$ | 87 051.137 (070)[e] | -11.32 | -1.42 | 11.4 |
| 3 | ±2 | ∓1 | $E_2$ | 87 019.805 (070) | - 1.64 | -0.21 | -32.1 |
| 3 | ±3 | 0 | $A_1+A_2$ | 87 032.195 (070) | - 2.28 | -0.29 | -26.1 |
| 3 | ±3 | ±1 | $E_4$ | not observed | | | 21.1 |
| 3 | ±3 | ∓1 | $E_4$ | 87 022.707 (070)[f] | - 2.51 | -0.31 | -22.1 |
| 4 | ±1 | 0 | $E_1$ | 108 822.733 (100) | -11.54 | -1.15 | 8.3 |
| 4 | ±1 | ±1 | $E_2$ | 108 798.227 (100)[f] | - 5.77 | -0.58 | - 8.2 |
| 4 | ±1 | ∓1 | $E_3$ | 108 776.348 (100)[f] | - 2.09 | -0.21 | -32.9 |
| 4 | ±2 | 0 | $E_1$ | 108 806.174 (100) | - 5.10 | -0.51 | -11.1 |
| 4 | ±2 | ±1 | $E_3$ | 108 812.043 (200) | -14.15 | -1.42 | 11.4 |
| 4 | ±2 | ∓1 | $E_2$ | 108 772.834 (100) | - 2.07 | -0.21 | -32.1 |
| 4 | ±3 | 0 | $A_1+A_2$ | 108 788.363 (100) | - 2.83 | -0.28 | -26.1 |
| 4 | ±3 | ±1 | $E_4$ | not observed[g] | | | 21.1 |
| 4 | ±3 | ∓1 | $E_4$ | 108 776.348 (100)[f] | - 3.27 | -0.33 | -22.1 |
| 4 | ±4 | 0 | $E_1$ | 108 769.865 (100) | - 2.21 | -0.22 | -33.4 |
| 4 | ±4 | ±1 | $E_2$ | 108 824.246 (150) | -10.98 | -1.10 | 5.2 |
| 4 | ±4 | ∓1 | $E_3$ | 108 780.815 (100) | - 6.92 | -0.69 | - 5.3 |

a - Except as noted, the frequencies were measured in the current work.

b - $\delta \equiv$ observed value minus that calculated from the constants in Table I.

c - $\delta B_3 \equiv \delta/[2(J+1)]$

d - These frequencies were taken from Ref. (8). No errors were given in the original work; the errors shown were assumed for the current comparison.

e - Stark effect studies confirm the K assignment.

f - This measured value falls close to two different predictions. Neither assignment can be ruled out

g - A weak line was observed at 108 859.39 (30) MHz with $\delta$ = -6.95 MHz. However, the resulting $\delta B$ is in sharp disagreement with the dependence on $(E_T^{(0)} - V_3^{eff})$ shown by the other transitions.

For a specific $v$ and $K$, the unweighted average over $\sigma$ of $\langle \Omega_p \rangle_{v K \sigma}$ can be calculated from Eqs. (16) and (17):

$$\overline{\langle \Omega_{+1} \rangle}_{vK} = a_0^{(\Omega)} + \sum_{n=3,6,9}^{\infty} a_n^{(\Omega)} \cos(2\pi n K \tilde{\rho}/3) \tag{18a}$$

$$\overline{\langle \Omega_{-1} \rangle}_{vK} = \sum_{n=3,6,9}^{\infty} a_n^{(\Omega)} \sin(2\pi n K \tilde{\rho}/3). \tag{18b}$$

TABLE IV

Pure Rotational Frequencies for $CH_3{}^{28}SiH_3$ in the ($v = 4$) Torsional Level (assignments tentative)

| Lower State J | K | σ | Γ | Observed Value[a] (MHz) | δ[b] (MHz) | $\delta B_4$[c] (MHz) | $E_T^{(0)} - V_3^{eff}$ ($cm^{-1}$) |
|---|---|---|---|---|---|---|---|
| 0 | 0 | 0 | $A_1$ | 21 737.82 (10)[d] | - 0.59 | -0.30 | 60.0 |
| 0 | 0 | ±1 | $E_4$ | 21 743.22 (10)[d] | - 2.18 | -1.09 | 137.2 |
| 1 | ±1 | 0 | $E_1$ | 43 485.61 (10)[d] | - 1.51 | -0.38 | 77.0 |
| 1 | ±1 | ±1 | $E_2$ | 43 493.00 (10)[d] | - 2.68 | -0.67 | 102.5 |
| 1 | ±1 | ∓1 | $E_3$ | 43 474.67 (10)[d] | - 7.57 | -1.89 | 174.9 |
| 3 | ±1 | 0 | $E_1$ | 86 969.80 (10)[e] | - 2.46 | -0.31 | 77.0 |
| 3 | ±1 | ±1 | $E_2$ | 86 984.23 (10) | - 5.15 | -0.64 | 102.5 |
| 3 | ±1 | ∓1 | $E_3$ | 86 948.45 (20) | -14.07 | -1.76 | 174.9 |
| 3 | ±2 | 0 | $E_1$ | 86 965.34 (10)[g] | - 5.40 | -0.68 | 107.7 |
| 3 | ±2 | ±1 | $E_3$ | 86 978.92 (10) | - 2.29 | -0.29 | 72.8 |
| 3 | ±2 | ∓1 | $E_2$ | 86 969.80 (10)[e] | -12.95 | -1.62 | 168.9 |
| 3 | ±3 | 0 | $A_1+A_2$ | 86 945.76 (10)[f] | - 9.23 | -1.15 | 143.0 |
| 3 | ±3 | ±1 | $E_4$ | 86 945.76 (10)[f] | + 0.06 | +0.01 | 60.6 |
| 3 | ±3 | ∓1 | $E_4$ | not observed | | | 131.5 |
| 4 | ±1 | 0 | $E_1$ | 108 710.26 (10)[f] | - 3.20 | -0.32 | 77.0 |
| 4 | ±1 | ±1 | $E_2$ | 108 728.62 (10) | - 6.25 | -0.63 | 102.5 |
| 4 | ±1 | ∓1 | $E_3$ | 108 683.50 (50) | -17.81 | -1.78 | 174.9 |
| 4 | ±2 | 0 | $E_1$ | 108 704.65 (10)[h] | - 6.93 | -0.69 | 107.7 |
| 4 | ±2 | ±1 | $E_3$ | 108 721.84 (10)[f] | - 2.81 | -0.28 | 72.8 |
| 4 | ±2 | ∓1 | $E_2$ | 108 710.26 (10)[f] | -16.35 | -1.64 | 168.9 |
| 4 | ±3 | 0 | $A_1+A_2$ | 108 677.30 (40) | -14.60 | -1.46 | 143.0 |
| 4 | ±3 | ±1 | $E_4$ | 108 680.28 (10) | + 0.03 | +0.00 | 60.6 |
| 4 | ±3 | ∓1 | $E_4$ | 108 732.64 (10) | -10.10 | -1.01 | 131.5 |
| 4 | ±4 | 0 | $E_1$ | 108 649.30 (40) | -19.58 | -1.96 | 181.0 |
| 4 | ±4 | ±1 | $E_2$ | 108 687.10 (40) | - 3.34 | -0.33 | 81.4 |
| 4 | ±4 | ∓1 | $E_3$ | 108 742.31 (10) | - 5.75 | -0.58 | 97.4 |

a - Except as noted, the frequencies were measured in the current work.

b - $\delta \equiv$ observed value minus that calculated from the constants in Table I.

c - $\delta B_4 \equiv \delta/[2(J+1)]$

d - These frequencies were taken from Ref. (8). No errors were given in the original work; the errors shown here were assumed for the current comparison.

e - Stark effect studies indicate the intensity is at least dominated by the (K = ±1) assignment. However, the (K = ±2) transition, which is calculated to be weaker by a factor ~2, could also be present. Both predicted frequencies fit the analysis reasonably well.

f - This measured value falls close to two different predictions. It is considered that both assignments are equally likely to be correct.

g - A second line was observed at 86 961.92 (10) MHz with $\delta$ = -8.82 MHz, but it is considered to be a poorer choice for this assignment.

h - A second line was observed at 108 700.53 (10) MHz with $\delta$ = -11.05 MHz, but is considered to be a poorer choice for this assignment.

For the ground torsional state and the current value of $s$ of 32, $|a_{n+1}/a_n| \sim 1/3000$. It is clear then, that to excellent approximation,

$$\overline{\langle \Omega_p \rangle}_0 = a_0^{(\Omega)} \qquad (p = +1) \tag{19a}$$

$$= 0 \qquad (p = -1). \tag{19b}$$

The subscript $K$ on the average has been dropped because, within the context of the approximation, the averages are independent of $K$.

For each $J$, the barrier anticrossings can yield two ($K = \pm 1 \leftrightarrow \mp 1$) splittings:

$$\nu_{EE} \equiv E(0, J, \pm 1, \mp 1) - E(0, J, \mp 1, \mp 1) \tag{20a}$$

$$\nu_{EA} \equiv E(0, J, \pm 1, \mp 1) - E(0, J, \mp 1, 0). \tag{20b}$$

Absolute measurements were made for $1 \leqslant J \leqslant 6$, and relative measurements were made of $\nu_{EE}(J = 2) - \nu_{EE}(J = 5)$ and of $\nu_{EA}(J = 2) - \nu_{EA}(J = 5)$. The results are summarized in Table II of Paper II.

For each $J$, the information contained in the two frequencies can be expressed as

$$\nu_{EA}/\nu_{EE} = \frac{1}{2}\{1 + \sqrt{3}\cot[2\pi\tilde{\rho}/3]\}\{1 + 2\sqrt{3}(A_2/A_1)\sin[(2\pi/3)(1 + \tilde{\rho})] + (\sqrt{3}/2)(B_1/A_1)\operatorname{cosec}[(2\pi/3)(1 - \tilde{\rho})]\operatorname{cosec}[2\pi\tilde{\rho}/3]\} \tag{21a}$$

$$-\frac{2}{3}(\nu_{EA}^2 + \nu_{EE}^2 - \nu_{EA}\nu_{EE})^{1/2} = A_1 + A_2\cos(2\pi\tilde{\rho}/3)\{1 - 4[\sin(2\pi\tilde{\rho}/3)]^2\}. \tag{21b}$$

In the quartic analysis in use for the beam data,

$$A_n = [\tilde{V}_3 + F_{3J}J(J + 1) + \tilde{F}_{3K}]a_n^{(3\alpha)} + \tilde{V}_6 a_n^{(6\alpha)} + [\tilde{F} + \tilde{\xi} - D_{Jm}J(J + 1) - D_{Km}]a_n^{(2)} - D_m a_n^{(4)} \qquad n = 1, 2 \tag{22a}$$

$$B_1 = -[d_J J(J + 1) + d_K]a_1^{(1)} - d_m a_1^{(3)}. \tag{22b}$$

In the superscripts on the $a_n$, $(3n\alpha)$ refers to $(1/2)(1 - \cos 3n\alpha)$ and $(n)$ refers to $p^n$. Equation (21) is a higher-order form of Eq. (13) of Paper II. In the correction terms in Eq. (21), the expression for $A_n$ can be simplified to

$$A_n = \tilde{V}_3 a_n^{(3\alpha)} + \tilde{F}a_n^{(2)} \qquad n \geqslant 2. \tag{23}$$

Equation (21a) gives a very accurate value for $\tilde{\rho}$. The two correction terms are small enough that $A_1$ and $A_2$ can be calculated to sufficient accuracy from rather approximate values of $\tilde{V}_3$ and $\tilde{F}$. In $B_1$, the $J$-dependent term is negligible, as can be shown from the value of $d_J$ obtained from the microwave data. The upper limit obtained from the combined fit for the other terms in $B_1$ shows that an error of at most 35 ppm is introduced into $\tilde{\rho}$ by setting $B_1 = 0$. This is negligible compared to errors from other sources. Furthermore, since the experimental splittings enter only as a ratio, the error in the dipole moment does not affect Eq. (21a). As a result, the value of $\tilde{\rho}$ obtained from Eq. (21a) is very insensitive to all other molecular constants. It is clear, then, why $\tilde{\rho}$ was chosen as a fitting parameter.

From Eq. (21b), the coefficient $A_1$ can be determined since $\tilde{\rho}$ is well known and $A_2$ again can be calculated to the required accuracy. From measurements of $A_1$ for a variety of $J$'s, one can determine the limit $L$ as $J \to 0$ and the derivative $S$ with respect to $J(J + 1)$.

$$L = [\tilde{V}_3 + \tilde{F}_{3K}]a_1^{(3\alpha)} + V_6 a_1^{(6\alpha)} + [\tilde{F} + \tilde{\xi} - D_{Km}]a_1^{(2)} - D_m a_1^{(4)} \tag{24a}$$

$$S = F_{3J}a_1^{(3\alpha)} - D_{Jm}a_1^{(2)}. \tag{24b}$$

Studies of the rotational anticrossings $(J, K, \sigma) = (1, \pm 1, \sigma) \leftrightarrow (2, 0, \sigma')$ yielded four splittings of the form

$$\nu_{\sigma\sigma'} = E(0, 1, \pm 1, \sigma) - E(0, 2, 0, \sigma'). \tag{25}$$

The results are given in Table II of Paper II. As in the barrier anticrossings, the contribution from Fourier coefficients with $n \geq 2$ can be corrected for without increasing the errors. If these coefficients are made, then the four splittings can be written

$$\nu_{\sigma\sigma'} = X_0 + X_1 \cos[(2\pi/3)(\tilde{\rho} - \sigma)] - Y_1 \sin[(2\pi/3)(\tilde{\rho} - \sigma)] - X_1' \cos[(2\pi/3)\sigma']. \tag{26}$$

The $J$-dependent contributions to the coefficients can be obtained from the microwave data to yield the corresponding $(J \rightarrow 0)$ limits.

$$\hat{X}_0 = \tilde{A} - D_K + \tilde{F}_{3K} a_0^{(3\alpha)} - D_{Km} a_0^{(2)} \tag{27a}$$

$$\hat{X}_1 = L \tag{27b}$$

$$\hat{Y}_1 = d_K a_1^{(1)} + d_m a_1^{(3)} \tag{27c}$$

$$\hat{X}_1' = \tilde{V}_3 a_1^{(3\alpha)} + [\tilde{F} + \tilde{\zeta}] a_1^{(2)} - D_m a_1^{(4)}. \tag{27d}$$

$\hat{Y}_1$ is insignificant here.

The information in the two types of anticrossings can now be deduced from Eqs. (24) and (27). If $D_K$ is taken from the force field (*23*) and the average defined in Eq. (19) is used, then $\hat{X}_0$ yields

$$A^{\text{eff}} = \tilde{A} - D_{Km}\overline{\langle \mathbf{p}^2 \rangle_0} + \tilde{F}_{3K}\overline{\left\langle \frac{1}{2}(1 - \cos 3\alpha) \right\rangle_0}. \tag{28}$$

Both $\tilde{\zeta}$ and $D_m$ can be set to zero because they cannot be determined. If $F_{\text{eff}}$ is calculated by using $A_{\text{eff}}$ and $\tilde{\rho}$ in Eq. (9), then $\hat{X}_1'$ can be inserted in Eq. (27d) to obtain the effective height of the potential $V_3^{\text{eff}}$. Further,

$$(\hat{X}_1 - \hat{X}_1') = \tilde{F}_{3K} a_1^{(3\alpha)} - D_{Km} a_1^{(2)} \tag{29a}$$

$$= -a_1^{(2)} D_{Km}^{\text{eff}}, \tag{29b}$$

where

$$D_{Km}^{\text{eff}} = D_{Km} + \lambda \tilde{F}_{3K} \tag{30a}$$

and

$$\lambda = -a_1^{(3\alpha)}/a_1^{(2)}. \tag{30b}$$

This demonstrates the origin of the three effective parameters in Table IV of Paper II; Eqs. (16) of Paper II have now been derived. The anticrossing data provide a fourth piece of information, namely the $J$ dependence $S$ in Eq. (24b) of the barrier anticrossing measurements.

Two types of "effective values" have been now introduced, one labeled with a tilde and another labeled with the superscript *eff*. The difference between the two should be kept clearly in mind. The tilde indicates the particular linear combination of molecular constants that arises from a transformation or a redundancy and cannot

be separated. This type of inseparability is similar to that first pointed out by Watson (*24*) for molecular centrifugal distortion constants. On the other hand, the superscript *eff* indicates that the particular linear combination of molecular constants cannot be separated because of the limitations of the data set. For example, if $A^{\text{eff}}$ could be measured for three different torsional levels, then $\tilde{A}$, $D_{Km}$, and $\tilde{F}_{3K}$ could be separated.

## V. ANALYSIS AND DISCUSSION

### *1. Spectra with $v \leqslant 2$*

A least-squares analysis was carried out on the 72 rotational frequencies for $v \leqslant 2$ in Table II and the 15 anticrossing measurements for $v = 0$ in Table II of Paper II. The 14 independent constants obtained in the best fit by direct diagonalization (Method III) are given in Table I here. For each rotational transition, the difference $\delta$ between the observed and calculated values is given in the current Table II. For the anticrossing splittings, these differences are not listed, but do not differ significantly from those given in Table II of Paper II. The overall fit is good, with a $\chi^2$ of 44 for 73 *df*. The only lines which show any indication of a possible systematic error are those in the ($J = 2 \leftarrow 1$) spectrum, where the experimental error was assumed to be 100 kHz in the absence of error estimates in the original work (*8*). With Method II, it was shown that the fit cannot be improved by including more constants from Eqs. (5) and (10). As each additional parameter was tested, it proved to be undeterminable and/or did not improve the fit significantly. These parameters were therefore fixed at zero in the Table I model.

The current model differs from the one used in Paper II in that now $H_{Jmm}$, $H_{JKm}$, $H_{JJm}$, and $F_{6J}$ are included, while $F_{9J}$ is excluded. In Paper II, with the limited microwave data available, $F_{9J}$ was used rather than $F_{6J}$, in spite of the fact that $F_{6J}$ is expected to be larger. This step was required to match the $J$ dependence of both the rotational frequencies and the anticrossing splittings.[6] Now with frequencies from much higher values of $J$, it is possible to determine three $H$'s and reproduce both $J$ dependences with $F_{6J}$. If the current data set is analyzed using $F_{9J}$ instead of $F_{6J}$, the resulting best fit constants agree with those obtained in Paper II. However, because $F_{6J}$ is used here, there are small changes in $A^{\text{eff}}$, $B$, $F_{3J}$, and $D_{Jm}$. These changes are a measure of the model errors in these parameters due to the fact that the sextic constants are entirely empirical. For example, although the current data cannot determine $\tilde{V}_6$ or $\tilde{\zeta}$, computer experiments show that the introduction of these constants can change the $J$ dependence, particularly at the sextic level, through their influence on the basis functions.

With the larger data set now available, the least-squares errors in the constants in Table I are improved as compared with the results in Paper II, particularly for the constants associated with $J$-dependent matrix elements. In spite of this, it is very difficult to isolate the true values of the leading parameters. Attempts to separate $A^{\text{eff}}$ and $D_{KM}^{\text{eff}}$ into $\tilde{A}$, $D_{Km}$, and $\tilde{F}_{3K}$ essentially reproduced Table V of Paper II because these constants are determined almost entirely from the anticrossing splittings. The

[6] This use of $F_{9J}$ rather than $F_{6J}$ also occurred in a similar experiment on $CH_3SiF_3$ (*25*).

analysis yielded $\tilde{A}$ = 56 179 (75) MHz and $\tilde{V}_3$ = 592.2 (1.0) $cm^{-1}$. These two values still contain contributions from other terms, first through Eqs. (8b) and (13b), and second through the fact that various constants have been fixed at zero. The contributions are negligible compared to the error in $\tilde{A}$, but may be significant for $\tilde{V}_3$.

The difference $(\tilde{\rho} - \rho)$ as given in Eq. (8a) may be large compared to the least-squares error of 140 ppm. When $\tilde{A}$ and $\tilde{\rho}$ are used to calculate the moment of inertia $I_\alpha$ of the methyl top, it is found that $I_\alpha$ = 3.165(5) amu-Å$^2$. This is in close agreement with the value of 3.170(2) amu-Å$^2$ obtained recently from similar experiments on $CH_3SiF_3$ (*25*). The agreement indicates that $|\tilde{\rho} - \rho| \leqslant 0.1\%$.

The values obtained for $D_J$ and $D_{JK}$ from the force field are 11.0 and 35.3 kHz, respectively (*23*). These are in reasonable agreement with the measured values given in Table I. Although both will be contaminated with sextic effects, the differences between the Table I values and the force field values should be dominated by uncertainties in the force field. These differences indicate the order of the discrepancy to be expected in the force field value assumed here for $D_K$. The values of $D_J$ and $D_{JK}$ assumed in Paper II were taken from a preliminary analysis of the current data.

### 2. *Spectra with $v = 3$ and $v = 4$*

The data for the higher torsional levels indicate that the existing model (*2, 3, 16*) must be modified for the higher torsional levels. The ($v = 3$) data were considered first. All attempts to include the ($v = 3$) data in the fit failed. Regardless of which group of constants is added to those in the best fit model of Table I, the $\chi^2$ remained two orders of magnitude larger than its value for the ($v \leqslant 2$) data set. In these fits, the magnitude of the (observed–calculated) values was typically 1 MHz for the ($v = 3$) lines as compared to the experimental error of ~0.1 MHz.

To investigate the disagreement further, the difference $\delta$ between the measured values and the frequencies calculated from Table I were determined along with the differences between the torsional energy $E_T^{(0)}$ calculated from Table I and $V_3^{\text{eff}}$. As can be seen from Table III, $E_T^{(0)}$ and $\delta$ show unusual patterns. For each $K$ except $K = 0$, the set of three torsional sublevels includes one which is well below the barrier top, a second which is somewhat closer to the top but still below, and a third which is above. The barrier top falls roughly midway between the upper two levels, For each such triplet, $|\delta|$ goes up by greater than or approximately a factor of 2 for each of the two steps up in energy.

For each line, $\delta B_3 \equiv \delta/[2(J + 1)]$ was calculated. As can be seen from Table III, $\delta B_3$ is a function of ($K$, $\sigma$), but not of $J$. This shows that each ($K$, $\sigma$) sublevel has an effective $B$ value. For each ($K$, $\sigma$), a mean $\overline{\delta B_3}$ was calculated by averaging over the $J$ values for which measurements were made. In Fig. 1, $\overline{\delta B_3}$ is shown to be a remarkably smooth function of $E_T^{(0)}$.

In spite of the fact that $|\delta|$ is over 10 MHz for many levels, there can be no doubt that the identification is correct. The evidence is conclusive, including arguments based on the clear separation of lines of different $v$ for $v < 4$, Stark effect measurements for two lines, and close agreement among the $\delta B_3$ for different $J$ but the same ($K$, $\sigma$). The smooth dependence of $\overline{\delta B_3}$ on $E_T^{(0)}$ is itself confirmation of the identification. It should be emphasized that the point with the largest $|\delta B_3|$ has ($K = 0$, $\sigma = 0$), for

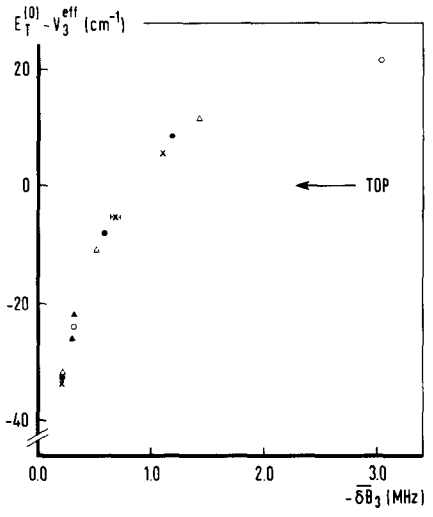


FIG. 1. Plot for ($v$ = 3) of the average discrepancy $\overline{\delta B}_3$ in the $B$ value for each ($K$, $\sigma$) as a function of the torsional energy difference ($E_T^{(0)} - V_3^{eff}$) from the top of the barrier. The typical error bar shown takes into account the error in the prediction. ○ for $|K|$ = 0; ● for $|K|$ = 1; △ for $|K|$ = 2; ▲ for $|K|$ = 3, and × for $|K|$ = 4.

which the experimental frequency has been measured twice earlier (*2, 5, 8*) and checked again here.

The corresponding assignment for ($v$ = 4) in Table IV is much less firm. The reasons for the difficulty are given in Section III. For ($K$ = 0), the identification is virtually unambiguous, primarily because of the simplicity of the ($J = 1 \leftarrow 0$) spectrum. For ($K = \pm 1$), the assignment is also virtually firm, primarily because three lines have been measured for three different values of $J$ including the relatively simple ($J = 2 \leftarrow 1$). For $K = \pm 2$, $\pm 3$, and $\pm 4$, the identification was made by using Fig. 2. The mean $\overline{\delta B_4}$ was calculated for $K$ = 0 and $K = \pm 1$, and then plotted against $E_T^{(0)} - V_3^{eff}$. As with ($v$ = 3), a smooth functional form is obtained. It was then assumed that the other $K$ values would fall near the same curve. As can be seen from Fig. 2, the resulting $\overline{\delta B_4}$ are consistent with this assumption. Furthermore, with the exception of the two lines indicated in the footnotes of Table IV and one very weak feature, the resulting assignment accounts for all the lines within the ranges spanned by the ($v$ = 4) frequencies. As was the case for ($v$ = 3), the largest $\overline{\delta B_4}$ occur for the highest energy; the discrepancies range from a few hundred kilohertz for low energy to almost 2 MHz at the high end.

For both ($v$ = 3) and ($v$ = 4), $\delta B_v$ shows no simple functional dependence on $K$ or $\sigma$. For example, for ($v$ = 3), ($K$ = 0, $\sigma$ = 0) has the largest $|\delta B|$ while ($K$ = 0, $\sigma = \pm 1$) has one of the smallest. The levels with the largest $|\delta B|$ for ($v$ = 3) have the smallest for ($v$ = 4). This apparently follows from the fact that the order of $E_T^{(0)}$ with respect to ($K$, $\sigma$) is reversed when $v$ goes from 3 to 4. There is no obvious correlation between $\delta B$ and the symmetry of the states.

It is clear that the origin of the $\delta B$ cannot lie in a complicated combination of

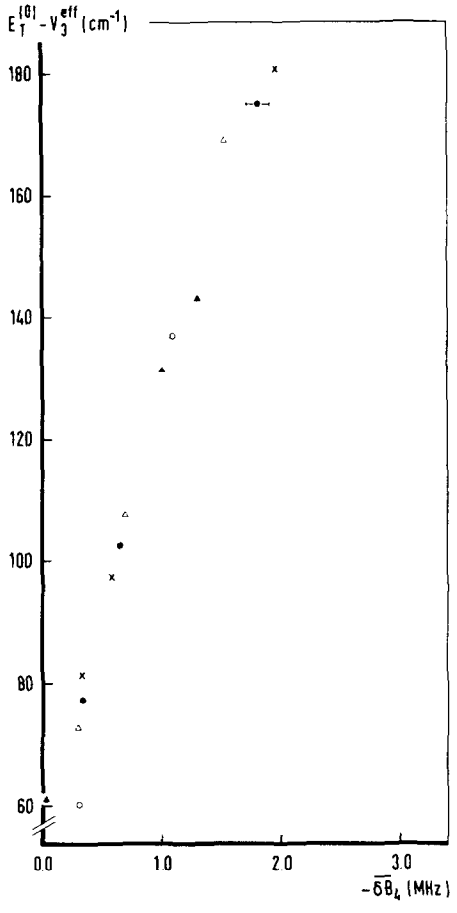


FIG. 2. Plot for ($v$ = 4) of the average discrepancy $\overline{\delta B_4}$ in the $B$ value for each ($K$, $\sigma$) as a function of the torsional energy difference ($E_T^{(0)} - V_3^{eff}$) from the top of the barrier. The typical error bar shown taken into account the error in the predictions. The assignments, particularly for $|K| > 1$, must be regarded as tentative. ○ for $|K| = 0$; ● for $|K| = 1$; △ for $|K| = 2$; ▲ for $|K| = 3$, and × for $|K| = 4$.

higher-order distortion effects. All the quartic constants in Eq. (5) involving the $J$ dependence have been determined. No sextic term could possibly correct for the magnitude of the effect which is observed at low $J$ and $K$.

There are two general types of mechanism which can account for the behavior illustrated in Figs. 1 and 2. The *first* is perturbation by a nearby vibrational state, which in this case would be the degenerate level ($v_{12} = 1$). The accepted fundamental frequency for this mode is $\nu_{12} = 545 \pm 3$ cm$^{-1}$ (*26, 27*). On the ($E_T^{(0)} - V_3^{eff}$) scale used in Figs. 1 and 2, this band origin falls at 52.5 cm$^{-1}$, which is 31 cm$^{-1}$ above the highest ($v = 3$) level. Figure 1 seems to require that the energy of the perturbing level be at most a few cm$^{-1}$ away from the highest ($v = 3$) level. In an effort to investigate this possible perturbation, a high resolution infrared study of the perpendicular band was undertaken very recently (*28*). Preliminary results indicate that $\nu_{12}$

is 20 $cm^{-1}$ lower than the published value. However, the smoothness of the dependence of $\delta B_3$ on energy suggests that the dominant mechanism for the model failure is not such vibrational mixing. If it were, then the matrix elements involved would have to be very insensitive to $K$ and $\sigma$. In any case, detailed analysis of the vibrational band should clarify this point.

It is clear from Figs. 1 and 2 that $\nu_{12}$ cannot be responsible for $\delta B_4$; after all, the ($v = 4$) levels closest to $\nu_{12}$ are perturbed the least. If $\nu_{12}$ is causing $\delta B_3$, then the level ($\nu_6 + \nu_{12}$) is probably responsible for $\delta B_4$; $\nu_6$ is the torsional mode.

The *second* possible explanation is either a perturbation which does not involve the vibrational degrees of freedom at all or involves only vibrational levels that are distant in energy. It is known from the computer searches that including higher terms in the potential such as $V_6$ does not remove the discrepancy. At first glance, it appears that the failure of these searches and similar ones involving such constants as $\zeta$ eliminates this second possibility. However, such a conclusion is not justified. As a counterexample, consider a distortion in the potential which requires many Fourier coefficients to be properly represented. The information available would then be insufficient to determine the several constants required and the least-squares fit would not converge. To solve the problem in this case would require a priori introduction of a suitable form for the distortion.

In $CH_3SiF_3$, a similar comparison between experiment and theory led to similar conclusions (*25*). For ($v = 3$), a $\delta B$ was observed with a larger magnitude for the levels whose energy falls above the top of the barrier. In that case, it was possible to resolve only ($\sigma = 0$) from ($\sigma = \pm 1$); the $K$ splitting was not resolved. Furthermore, no ($v = 4$) data were available. As a result, the information obtained on $\delta B$ was far more limited. However, it is clear that a similar type of effect is occurring and that the modification required of the Hamiltonian is not peculiar to methyl silane.

Work is continuing on $CH_3SiH_3$ in an effort to understand better the problem of internal rotation. Several different techniques are involved, including molecular beams. Fourier transform spectroscopy, and diode laser spectroscopy.

## VI. ISOTOPIC STUDIES

Pure rotational spectra in the ground torsional state were studied briefly for $^{12}CH_3{}^{30}SiH_3$, $^{12}CH_3{}^{29}SiH_3$, and $^{13}CH_3{}^{28}SiH_3$ in natural abundance. The frequencies measured are listed in Table V. The three ($J = 1 \leftarrow 0$) lines had been measured previously (*20, 29*). Small differences exist with the current values, but these are not considered to be significant since no experimental errors were assigned to the original measurements.

The present data for $^{12}CH_3{}^{30}SiH_3$ have been used in two earlier works in this series. First, a rigid rotor analysis was used to determine that the effective $B$ value $B_0$ for ($v = 0$) is 10 806.90 (20) MHz. This constant is $\hat{B}$ ($v = 0$, $K$, $\sigma$) averaged over $K$ and $\sigma$ since the torsional splitting cannot be resolved for $v = 0$ with conventional microwave methods. The corresponding number for the parent species $^{12}CH_3{}^{28}SiH_3$ is 10 968.964 (50) MHz. Both values of $B_0$ were used in treating the Stark effect in Paper I. Second, the true value of $B$ as defined in Eq. (15) measured here for $^{12}CH_3{}^{30}SiH_3$ was used

TABLE V

Pure Rotational Frequencies (in MHz) for Various Isotopic Forms of Methyl Silane in the ($v$ = 0) State

| Isotope | Lower State[a] J | K | Observed Value | Observed -Calculated | Previous Measurements[b] |
|---|---|---|---|---|---|
| $^{12}CH_3{}^{30}SiH_3$[c] | 0 | 0 | 21 613.701 (030) | -0.055 | 21 613.06 Ref.(20) |
| | 3 | 1 | 86 452.117 (100) | 0.008 | |
| | 3 | 2 | 86 451.005 (100) | -0.039 | |
| | 3 | 3 | 86 449.421 (100) | 0.184 | |
| $^{12}CH_3{}^{29}SiH_3$[d] | 0 | 0 | 21 770.978 (030) | -0.010 | 21 771.08 Ref.(20) |
| | 3 | 1 | 86 080.980 (070) | -0.057 | |
| | 3 | 2 | 86 079.950 (070) | -0.022 | |
| | 4 | 1 | 108 849.343 (070) | -0.023 | |
| | 4 | 2 | 108 848.113 (070) | 0.078 | |
| | 4 | 3 | 108 845.767 (100) | -0.009 | |
| | 4 | 4 | 108 842.776 (200) | 0.194 | |
| $^{13}CH_3{}^{28}SiH_3$[e] | 0 | 0 | 21 212.736 (030) | | 21 213.04 Ref.(29) |

a - The $\sigma$ splitting was not resolved. The fits were made by setting the calculated frequency equal the average over $\sigma$ weighted by the intensities.

b - No experimental errors were quoted in the original works.

c - The fit was made to these microwave data and the anticrossing splittings in Table II of Paper II. B, A, $\rho$ and $V_3$ were varied; all other constants were fixed at the values for the parent species.

d - Only B was varied. Small corrections for the isotopic substitution were made to the values of A and $\rho$ of the Si-28 species. The remaining constants were fixed at the Si-28 values.

e - Only B was varied. All other constants were fixed at the C-12 values.

in Paper II along with the anticrossing measurements to obtain $A^{\text{eff}}$, $V_3^{\text{eff}}$, and $\tilde{\rho}$. The isotopic changes in these parameters are discussed in Section VI of Paper II.

Here the data is used along with existing measurements on $^{12}CH_3{}^{28}SiD_3$ (*8*) and $^{12}CD_3{}^{28}SiH_3$ (*9*) to obtain a structure that is based only on symmetric top rotational constants that have been corrected for internal rotation effects. The rotational constants and moments of inertia used are summarized in Table VI for all six species used, including the parent. For $^{12}CH_3{}^{28}SiD_3$, the nine observed frequencies (*8*) for $v \leqslant 2$ were analyzed by fitting $B$, $D_{Jm}$, $F_{3J}$, $F_{6J}$, and $d_J$. For $^{12}CD_3{}^{28}SiH_3$, the four frequencies (*9*) for $v \leqslant 2$ were analyzed by fitting $B$, $D_{Jm}$, $F_{3J}$, and $F_{6J}$; $d_J$ did not enter because $K = 0$ for all the spectra. In both cases, $A^{\text{eff}}$ and $\tilde{\rho}$ were corrected for deuteration and left fixed. The distortion constants that were not varied were fixed at the values for the parent species. For the on-axis isotopic substitutions, the analysis methods are

TABLE VI

Rotational Constants and Moments of Inertia for Some Symmetric Top Isotopic Forms of Methyl Silane[a,b]

| Isotope | B (MHz) | $I_b$(amu - Å$^2$) |
|---|---|---|
| $^{12}CH_3{}^{28}SiH_3$ | 10 986.095 (5) | 46.0017 (2) |
| $^{12}CH_3{}^{29}SiH_3$ | 10 902.710 (10) | 46.3535 (4) |
| $^{12}CH_3{}^{30}SiH_3$ | 10 824.095 (10) | 46.6902 (4) |
| $^{13}CH_3{}^{28}SiH_3$ | 10 623.585 (15) | 47.5714 (7) |
| $^{12}CD_3{}^{28}SiH_3$[c] | 9 132.18 (10) | 55.3405 (60) |
| $^{12}CH_3{}^{28}SiD_3$[c] | 9 636.609 (50) | 52.4437 (28) |

a - For $^{12}CH_3{}^{28}SiH_3$, A = 56 179 (75) MHz and $I_a$ = 8.996 (12) amu - Å$^2$.

b - The moment of inertia $I_\alpha$ of the methyl top in $^{12}CH_3{}^{28}SiH_3$ is 3.165 (5) amu - Å$^2$.

c - B for $^{12}CH_3SiD_3$ and $^{12}CD_3{}^{28}SiH_3$ were obtained by analysing data taken from Ref. (8) and Ref. (9), respectively.

given in Table V. In all cases the final value of *B* was insensitive to the details of the model used.

In Table VII, the structure obtained is compared to that obtained from an analysis of 23 different isotopic species (*29, 30*), most of which were asymmetric rotors. This earlier analysis used a PAM treatment of internal rotation that included only the leading term, viz., the first term in Eq. (6). The two structures agree very well. The current structure calculation is a little more accurate, but of greater importance is the demonstration that the two different methods give consistent results.

TABLE VII

The Structure of Methyl Silane

| | | Present Work | Ref. (30)[a] |
|---|---|---|---|
| r(SiH) | Å | 1.482 (2) | 1.484 (5) |
| ∠(HCH) | degrees | 108.03 (11) | 108.00 (50) |
| r(CSi) | Å | 1.864 (1) | 1.867 (1) |
| r(CH) | Å | 1.095 (1) | 1.092 (5) |
| ∠(HSiH) | degrees | 108.49 (14) | 108.73 (50) |
| ∠(CSiH) | degrees | 110.41 (10) | 110.20 (50) |

a - These results were obtained in Ref. (30) by reanalysing the data in Ref. (29).

## ACKNOWLEDGMENTS

The current work could not have been undertaken without the generous cooperation of three different microwave laboratories. In this regard, the authors thank Mr. B. W. Statt, Dr. R. Jochemsen, and Dr. W. N. Hardy of the Physics Department, University of British Columbia; Mr. G. A. McRae and Dr. M. C. L. Gerry of the Chemistry Department, University of British Columbia; and Dr. Ch. Ryzlewicz, Dr. H.-U. Schütze-Pahlmann, and Dr. T. Törring of the Institut für Molekülphysik, Freie Universität Berlin. The authors are grateful to Dr. H. Jagannath and Dr. J. K. G. Watson for many fruitful discussions, and to Dr. A. Dymanus for his stimulating interest in the problem. Two of us (M. Wong and I. Ozier) express our appreciation to the Natural Sciences and Engineering Research Council of Canada for its support, and to the National Research Council of Canada for its hospitality while the manuscript was being completed. The authors also thank the North Atlantic Treaty Organization Research Grant Program for its support through Travel Grant 1454.

RECEIVED: June 14, 1983

## REFERENCES

1. W. L. MEERTS AND I. OZIER, *Phys. Rev. Lett.* **41,** 1109–1112 (1978).
2. D. KIVELSON, *J. Chem. Phys.* **22,** 1733–1739 (1954); *J. Chem. Phys.* **23,** 2230–2235 (1955); *J. Chem. Phys.* **27,** 980–980 (1957).
3. B. KIRTMAN, *J. Chem. Phys.* **37,** 2516–2539 (1962).
4. J. R. DURIG, Y. S. LI, AND C. C. TONG, *J. Mol. Struct.* **14,** 255–260 (1972).
5. D. R. LIDE, JR., D. R. JOHNSON, K. G. SHARP, AND T. D. COYLE, *J. Chem. Phys.* **57,** 3699–3703 (1972).
6. L. C. KRISHER, W. A. WATSON, AND J. A. MORRISON, *J. Chem. Phys.* **61,** 3429–3433 (1974).
7. P. CAHILL AND S. BUTCHER, *J. Chem. Phys.* **35,** 2255–2256 (1961).
8. E. HIROTA, *J. Mol. Spectrosc.* **43,** 36–64 (1972).
9. C. S. EWIG, W. E. PALKE, AND B. KIRTMAN, *J. Chem. Phys.* **60,** 2749–2758 (1974).
10. I. OZIER AND W. L. MEERTS, *Phys. Rev. Lett.* **40,** 226–229 (1978).
11. I. OZIER AND W. L. MEERTS, *Canad. J. Phys.* **59,** 150–171 (1981).
12. I. OZIER AND W. L. MEERTS, *J. Mol. Spectrosc.* **93,** 164–178 (1982).
13. W. L. MEERTS AND I. OZIER, *J. Mol. Spectrosc.* **94,** 38–54 (1982).
14. R. M. LEES AND J. G. BAKER, *J. Chem. Phys.* **48,** 5299–5318 (1968).
15. R. M. LEES, *J. Chem. Phys.* **59,** 2690–2697 (1973).
16. C. C. LIN AND J. D. SWALEN, *Rev. Mod. Phys.* **31,** 841–892 (1959).
17. E. R. COHEN AND B. N. TAYLOR, *J. Phys. Chem. Ref. Data* **2,** 663–739 (1973).
18. Y. Y. KWAN AND D. M. DENNISON, *J. Mol. Spectrosc.* **43,** 291–319 (1972).
19. F. ROHART, *J. Mol. Spectrosc.* **57,** 301–311 (1975).
20. D. R. LIDE, JR., AND D. K. COLES, *Phys. Rev.* **80,** 911–911 (1950).
21. B. W. STATT, W. N. HARDY, AND R. JOCHEMSEN, *Canad. J. Phys.* **58,** 1326–1340 (1980).
22. CH. RYZLEWICZ AND T. TÖRRING, *Chem. Phys.* **51,** 329–334 (1980); H.-U. SCHÜTZE-PAHLMANN, Ph.D. thesis, Freie Universität, Berlin, 1981.
23. E. A. CLARK AND A. WEBER, *J. Chem. Phys.* **45,** 1759–1766 (1966).
24. J. K. G. WATSON, *J. Chem. Phys.* **46,** 1935–1949 (1967).
25. W. L. MEERTS AND I. OZIER, *Chem. Phys.* **71,** 401–415 (1982).
26. R. E. WILDE, *J. Mol. Spectrosc.* **8,** 427–454 (1962).
27. M. RANDIC, *Spectrochim. Acta* **18,** 115–122 (1962).
28. I. OZIER, H. JAGANNATH, AND J. W. C. JOHNS, *private communication.*
29. R. W. KILB AND L. PIERCE, *J. Chem. Phys.* **27,** 108–112 (1957).
30. L. PIERCE AND D. H. PETERSEN, *J. Chem. Phys.* **33,** 907–913 (1960).